THE JOURNAL OF PHYSICAL CHEMISTRY LETTERS
A JOURNAL OF THE AMERICAN CHEMICAL SOCIETY

pubs.acs.org/JPCL Letter

An Algebraic-Diagrammatic Construction for Vertex Corrections to the *GW* Self-Energy

Antoine Marie,* Johannes Tölle,* and Pierre-François Loos*

Cite This: *J. Phys. Chem. Lett.* 2026, 17, 8541−8551 Read Online

ACCESS | Metrics & More | Article Recommendations | Supporting Information

ABSTRACT: The *G*3*W*2 approximation—the second-order self-energy beyond *GW*—is known to violate some fundamental analytic properties of the self-energy. In particular, its lack of positive semidefiniteness leads to unphysical features such as negative spectral functions. In this work, we reformulate the *G*3*W*2 approximation within the algebraic-diagrammatic construction (ADC) framework. The resulting ADC-*G*3*W*2 formalism enforces the same analytic form as the exact self-energy, namely a spectral representation, and, consequently, guarantees positive semidefiniteness. Starting from the *GW* self-energy, we construct a hierarchy of ADC-based approximations of increasing sophistication, including ADC-2SOSEX, ADC(3)-*G*3*W*2, and a full ADC-*G*3*W*2 scheme. These methods can be interpreted as infinite resummations of vertex corrections to the self-energy, yielding Hermitian effective Hamiltonians whose diagonalization provides quasiparticle and satellite energies. This establishes a formal bridge between many-body perturbation theory formulated in terms of the screened interaction *W* and conventional ADC schemes based on the bare Coulomb interaction. The performance of these ADC-based approximations is gauged for valence ionization potentials and benchmarked against their parent method.

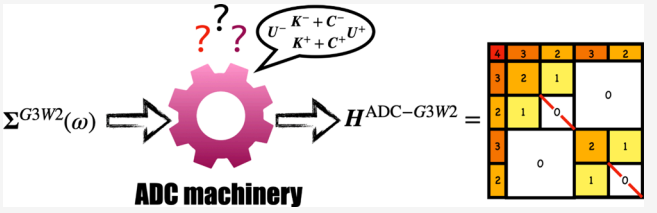

Many-body perturbation theory (MBPT)[1,2] has undergone rapid development in recent years.[3−7] Although historically rooted in condensed matter physics,[8−13] it has emerged as a viable and competitive framework for quantum chemical calculations on molecular systems.[14−23] In particular, MBPT-based approaches have become well-established tools for the computation of ionization potentials[23−35] and optical excitations[36−49] at a computational cost that remains affordable[50−63] while achieving an accuracy comparable to that of wave function methods.

Within this context, the *GW* approximation has proven especially successful.[3−5,64,65] In this approach, the one-body Green's function *G* is obtained through the Dyson equation

$$G^{-1} = G_0^{-1} - \Sigma \tag{1}$$

(where G_0 is the Hartree Green's function) by approximating the self-energy Σ as the product of *G* and the dynamically screened Coulomb interaction *W*

$$\Sigma^{GW} = iGW \tag{2}$$

where $W = v + W_P$ is conveniently decomposed into its bare (static) Coulomb part *v* and a (dynamic) polarizable contribution W_P. This self-energy is represented diagrammatically in the left panel of Figure 1. The *GW* approximation can be straightforwardly derived from Hedin's equations by retaining only the lowest-order contribution to the vertex function Γ. While this approximation captures a substantial fraction of dynamical correlation effects and provides a proper description of quasiparticle states in weakly correlated systems, it remains inadequate for multireference systems,[66,67] strongly correlated materials,[68−75] or multiparticle processes such as satellite excitations.[28,76,77]

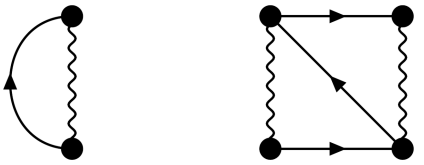

Figure 1. Diagrammatic representation of the *GW* (left) and *G*3*W*2 (right) self-energies. The solid and wiggly lines represent *G* and *W*, respectively.

Going beyond *GW* is done through the inclusion of vertex corrections, either in the self-energy Σ and/or in the polarizability *P* (which is used to compute *W*). Vertex corrections in the self-energy correspond to going beyond first order in the screened interaction *W* and are commonly referred to as outer-vertex corrections,[78−83] while vertex corrections in the polarizability improve the screening itself by incorporating interaction effects beyond the direct random-

Received: June 10, 2026
Revised: July 2, 2026
Accepted: July 9, 2026
Published: July 14, 2026

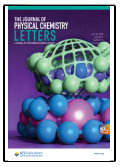

https://doi.org/10.1021/acs.jpclett.6c01904
J. Phys. Chem. Lett. 2026, 17, 8541−8551

phase approximation (RPA) and are known as inner-vertex corrections.[14,25,26,84−89] A growing body of evidence indicates that these two types of corrections should be treated on an equal footing:[52,76,90−108] the apparent success of standard GW often relies on a fortuitous cancellation of errors between Σ and P.[25,76,82,106,108] As a result, systematic improvements over GW necessitate the consistent inclusion of both inner- and outer-vertex corrections, thereby providing a more balanced and physically sound description of electronic correlation.

However, it is often unclear how to systematically improve each of these quantities in a controlled and reliable manner. For example, in the case of the self-energy, going beyond GW typically amounts to adding higher-order terms in the perturbative expansion of Σ with respect to W.[76] The leading correction beyond GW is provided by the second-order self-energy, commonly referred to as the $G3W2$ approximation[81−83,109]

$$\Sigma^{G3W2} = \Sigma^{GW} + i^2 GWGWG \tag{3}$$

This additional term is represented diagrammatically in the right panel of Figure 1. A natural approximation of this self-energy is obtained by discarding the computationally expensive $i^2 GW_pGW_pG$ contribution[82,83]

$$\Sigma^{2SOSEX} = \Sigma^{GW} + i^2 GvGvG + i^2 GW_pGvG + i^2 GvGW_pG \tag{4}$$

This computationally more affordable approximation that retains the dominant second-order exchange and screening effects beyond GW is referred to as the second-order screened exchange (2SOSEX) contribution.

Unfortunately, the convergence properties of such perturbative series are largely unknown, and the naive inclusion of higher-order contributions may lead to erratic or even deteriorated results. Moreover, truncated perturbative expressions may violate fundamental properties of the self-energy. For example, they are not guaranteed to have a spectral representation, i.e., the same analytic form as the exact self-energy,[110] or they might not be positive semidefinite (psd). This latter property of the self-energy is sufficient to ensure that the associated spectral function of G is positive.[111] These issues are not specific to perturbative expansions in terms of W, but were already recognized in early many-body perturbation theories formulated in terms of the bare Coulomb interaction v.[111]

Stefanucci and co-workers have shown, using diagrammatic techniques, how to complete an approximate self-energy into a psd approximation by adding a finite number of diagrams.[112−114] Recently, this scheme has been applied to the 2SOSEX approximation, and the performance of the resulting 2SOSEX-psd self-energy has been gauged for ionization potentials of molecules.[83] Note that the resulting psd self-energies obtained within this formalism do not necessarily admit a spectral representation.

The algebraic-diagrammatic construction (ADC) goes one step further, as it is specifically designed to complete an approximate self-energy into a form that preserves the analytic structure of the exact self-energy. This objective cannot, in general, be achieved by adding only a finite number of diagrams, as in the aforementioned scheme. Instead, ADC relies on infinite resummations of diagrammatic contributions to enforce this property. This scheme was originally applied to the perturbation expansion of the self-energy in terms of the Coulomb interaction, and this led to the ADC(n) family of approximations for the self-energy.[115−117]

In this work, we extend this idea by applying the ADC to the perturbative expansion of the self-energy in terms of W. Within this perspective, ADC can be interpreted as an infinite resummation of vertex corrections to the self-energy, yielding a hierarchy of ADC-based approximations that explicitly admit a spectral representation and are, hence, positive semidefinite.[117] This framework provides a route to improve upon GW through the inclusion of vertex corrections while maintaining fundamental analytic properties of the self-energy. A conceptually related, albeit distinct, strategy has recently been explored within the multichannel Dyson equation formalism[118,119] to construct a screened formulation based on the static limit of W.[120]

Importantly, the present ADC treatment addresses only the outer-vertex part of the problem. Identifying the appropriate inner-vertex corrections that should accompany this approach remains an open and essential question. As will be discussed in the concluding section, a balanced treatment of both contributions is expected to improve accuracy and reduce the reliance on error cancellation, thereby paving the way toward a more complete and predictive MBPT framework.

The nth-order ADC approximation for the self-energy, denoted ADC(n), is defined as being complete through nth order in the Coulomb interaction and having a spectral representation. This latter property is enforced by adding and resumming a well-defined subset of higher-order contributions. Solving the Dyson equation using an approximate ADC(n) self-energy is referred to as Dyson-ADC(n) in the literature.[117]

Formally, the ADC procedure starts from the exact spectral representation of the self-energy. The self-energy can be decomposed as

$$\boldsymbol{\Sigma}(\omega) = \boldsymbol{\Sigma}(\infty) + \boldsymbol{\Sigma}^{-}(\omega) + \boldsymbol{\Sigma}^{+}(\omega) \tag{5}$$

where $\boldsymbol{\Sigma}(\infty)$ is the static self-energy, while $\boldsymbol{\Sigma}^{-}(\omega)$ and $\boldsymbol{\Sigma}^{+}(\omega)$ are the lesser and greater, also known as hole and electron, branches of the dynamical part of the self-energy, respectively. The branches of the dynamical self-energy have the following *diagonal* spectral representation

$$\boldsymbol{\Sigma}^{\pm}(\omega) = (\boldsymbol{V}^{\pm})^{\dagger}\cdot(\boldsymbol{\omega} - \boldsymbol{\mathcal{E}}^{\pm})^{-1}\cdot\boldsymbol{V}^{\pm} \tag{6}$$

where $\boldsymbol{V}^{\pm}$ contains the so-called Dyson amplitudes, $\boldsymbol{\mathcal{E}}^{\pm}$ is a diagonal matrix gathering the poles of the self-energy in the lower/upper part of the complex plane, and $\boldsymbol{\omega} = \omega\mathbf{1}$. Upon unitary transformations $\boldsymbol{Q}^{\pm}$ such that

$$\boldsymbol{U}^{\pm} = \boldsymbol{Q}^{\pm}\cdot\boldsymbol{V}^{\pm} \quad \boldsymbol{K}^{\pm} + \boldsymbol{C}^{\pm} = \boldsymbol{Q}^{\pm}\cdot\boldsymbol{\mathcal{E}}^{\pm}\cdot(\boldsymbol{Q}^{\pm})^{\dagger} \tag{7}$$

one can go from the diagonal spectral representation to the equivalent *nondiagonal* ADC form

$$\boldsymbol{\Sigma}^{\pm}(\omega) = (\boldsymbol{U}^{\pm})^{\dagger}\cdot(\boldsymbol{\omega} - \boldsymbol{K}^{\pm} - \boldsymbol{C}^{\pm})^{-1}\cdot\boldsymbol{U}^{\pm} \tag{8}$$

where $\boldsymbol{K}^{\pm}$ are diagonal matrices corresponding to the zeroth-order approximation of the diagonal matrices $\boldsymbol{\mathcal{E}}^{\pm}$.

So far, the discussion has been formulated in terms of the exact self-energy. To construct the desired ADC(n) scheme, the matrices $\boldsymbol{U}^{\pm}$ and $\boldsymbol{C}^{\pm}$ are expanded perturbatively as

$$\boldsymbol{U}^{\pm} = \boldsymbol{U}^{\pm,(1)} + \boldsymbol{U}^{\pm,(2)} + \ldots \tag{9a}$$

$$\boldsymbol{C}^{\pm} = \boldsymbol{C}^{\pm,(1)} + \boldsymbol{C}^{\pm,(2)} + \ldots \tag{9b}$$

https://doi.org/10.1021/acs.jpclett.6c01904
J. Phys. Chem. Lett. 2026, 17, 8541−8551

The corresponding perturbative expansion of the self-energy branches then reads

$$\begin{aligned}\boldsymbol{\Sigma}^{\pm}(\omega) &= (\boldsymbol{U}^{\pm})^{\dagger}\cdot(\omega - \boldsymbol{K}^{\pm})^{-1}\cdot\sum_{k=0}^{\infty}[\boldsymbol{C}^{\pm}\cdot(\omega - \boldsymbol{K}^{\pm})^{-1}]^{k}\cdot\boldsymbol{U}^{\pm} \\ &= [\boldsymbol{U}^{\pm,(1)}]^{\dagger}\cdot(\omega - \boldsymbol{K}^{\pm})^{-1}\cdot\boldsymbol{U}^{\pm,(1)} \\ &\quad + [\boldsymbol{U}^{\pm,(2)}]^{\dagger}\cdot(\omega - \boldsymbol{K}^{\pm})^{-1}\cdot\boldsymbol{U}^{\pm,(1)} \\ &\quad + [\boldsymbol{U}^{\pm,(1)}]^{\dagger}\cdot(\omega - \boldsymbol{K}^{\pm})^{-1}\cdot\boldsymbol{U}^{\pm,(2)} \\ &\quad + [\boldsymbol{U}^{\pm,(1)}]^{\dagger}\cdot(\omega - \boldsymbol{K}^{\pm})^{-1}\cdot\boldsymbol{C}^{\pm,(1)}\cdot(\omega - \boldsymbol{K}^{\pm})^{-1}\cdot \\ &\quad \boldsymbol{U}^{\pm,(1)} + \ldots \end{aligned} \tag{10}$$

The perturbative expansions of blocks $\boldsymbol{U}^{\pm}$ and $\boldsymbol{C}^{\pm}$ are determined by explicitly identifying eq 10 with the corresponding perturbative expansion of the self-energy in powers of the bare Coulomb interaction.[117] Once determined, these quantities can be inserted into eq 8 to get the ADC(n) approximate self-energy.

Upon substitution into the Dyson equation, and owing to its structure [see eq 8], the problem can be reformulated as a Hermitian eigenvalue problem.[115−117] The eigenvalues of the resulting effective Hamiltonian correspond to the poles of the one-body Green's function, that is, the ionization potentials (IPs) and electron affinities (EAs) of the system. Note that, for each type of charged excitations, this effective Hamiltonian provides both quasiparticle and satellite energies.

The main idea of this work is to apply this procedure to the *G*3*W*2 self-energy, thereby completing it into an approximation, referred to as ADC-*G*3*W*2, that retains the analytic structure of the exact self-energy. The electron and hole branches of the *G*3*W*2 self-energy can both be written in terms of intermediate quantities as (see the Supporting Information for a detailed derivation)

$$\begin{aligned}\boldsymbol{\Sigma}^{\pm}(\omega) &= [\boldsymbol{U}_1^{\pm,(1)}]^{\dagger}\cdot(\omega - \boldsymbol{K}_1^{\pm})^{-1}\cdot\boldsymbol{U}_1^{\pm,(1)} \\ &\quad + [\boldsymbol{U}_1^{\pm,(2)}]^{\dagger}\cdot(\omega - \boldsymbol{K}_1^{\pm})^{-1}\cdot\boldsymbol{U}_1^{\pm,(1)} + [\boldsymbol{U}_1^{\pm,(1)}]^{\dagger} \\ &\quad \cdot(\omega - \boldsymbol{K}_1^{\pm})^{-1}\cdot\boldsymbol{U}_1^{\pm,(2)} \\ &\quad + [\boldsymbol{U}_1^{\pm,(1)}]^{\dagger}\cdot(\omega - \boldsymbol{K}_1^{\pm})^{-1}\cdot\boldsymbol{C}_1^{\pm}\cdot(\omega - \boldsymbol{K}_1^{\pm})^{-1}\cdot\boldsymbol{U}_1^{\pm,(1)} \\ &\quad + [\boldsymbol{U}_1^{\pm,(3)}]^{\dagger}\cdot(\omega - \boldsymbol{K}_1^{\pm})^{-1}\cdot\boldsymbol{U}_1^{\pm,(1)} \\ &\quad + [\boldsymbol{U}_1^{\pm,(1)}]^{\dagger}\cdot(\omega - \boldsymbol{K}_1^{\pm})^{-1}\cdot\boldsymbol{U}_1^{\pm,(3)} \\ &\quad + [\boldsymbol{U}_2^{\pm,(1)} + \boldsymbol{C}_{2/1}^{\pm}\cdot(\omega - \boldsymbol{K}_1^{\pm})^{-1}\cdot\boldsymbol{U}_1^{\pm,(1)}]^{\dagger} \\ &\quad \cdot(\omega - \boldsymbol{K}_2^{\pm})^{-1}\cdot[\boldsymbol{U}_2^{\pm,(1)} + \boldsymbol{C}_{2/1}^{\pm}\cdot(\omega - \boldsymbol{K}_1^{\pm})^{-1}\cdot \\ &\quad \boldsymbol{U}_1^{\pm,(1)}] \end{aligned} \tag{11}$$

The explicit expressions of all matrix elements for each branch will be detailed below. One can readily see that the *G*3*W*2 self-energy, when written in terms of these intermediate quantities, closely resembles the perturbative expansion of the self-energy in eq 10. Owing to this formulation, it becomes possible to identify the different contributions to the ADC blocks and to construct the corresponding ADC effective Hamiltonian based on the *G*3*W*2 self-energy. For clarity, we deliberately refrain from assigning perturbative orders to the various terms, as these can be misleading in the present context and are not required for the construction of the ADC scheme.

In the following, ϵ_p are the reference mean-field energies, Ω_ν are the direct RPA excitation energies, $X_{ia,\nu}$ and $Y_{ai,\nu}$ the elements of the corresponding eigenvectors, $\langle pq|rs\rangle$ are two-electron integrals in Dirac notations, and

$$M_{pq,\nu} = \sqrt{2}\sum_{ia}[\langle pa|qi\rangle X_{ia,\nu} + \langle pi|qa\rangle Y_{ai,\nu}] \tag{12}$$

are the *GW* effective integrals. (We refer the reader to ref 5 for more details.) Here, the indices p, q, r, s, ⋯ are used for arbitrary orbitals, i, j, k, l label the occupied orbitals, a, b, c, d denote the virtual orbitals, and μ, ν, ⋯ are used for combined occupied-virtual indices. All quantities are expressed in the spatial-orbital basis.

Retaining only the first term in $\boldsymbol{\Sigma}^{+}$ [see eq 11], together with its counterpart in $\boldsymbol{\Sigma}^{-}$, recovers the standard *GW* self-energy. The ADC identification procedure naturally begins from this contribution, which defines the leading terms of the diagonal matrices $\boldsymbol{K}^{-}$ and $\boldsymbol{K}^{+}$,

$$(\boldsymbol{K}_1^{-})_{i\nu,j\mu} = (\epsilon_i - \Omega_\nu)\delta_{ij}\delta_{\nu\mu} \tag{13a}$$

$$(\boldsymbol{K}_1^{+})_{a\nu,b\mu} = (\epsilon_a + \Omega_\nu)\delta_{ab}\delta_{\nu\mu} \tag{13b}$$

As usual, these contributions correspond to the inclusion of two-hole-one-particle (2h1p) and two-particle-one-hole (2p1h) configurations. In this case, the energies of these configurations are "dressed", as they are constructed from RPA excitation energies. The corresponding leading contributions to the coupling matrices are

$$(\boldsymbol{U}_1^{-,(1)})_{i\nu,q} = M^{*}_{qi,\nu} \tag{14a}$$

$$(\boldsymbol{U}_1^{+,(1)})_{a\nu,q} = M_{aq,\nu} \tag{14b}$$

which are likewise dressed quantities (i.e., *GW* effective integrals) in the present formalism. Once included in eq 8, solving the Dyson equation becomes equivalent to diagonalizing the following effective Hamiltonian[117]

$$\boldsymbol{H} = \begin{pmatrix} \boldsymbol{f} & (\boldsymbol{U}_1^{-})^{\dagger} & (\boldsymbol{U}_1^{+})^{\dagger} \\ \boldsymbol{U}_1^{-} & \boldsymbol{K}_1^{-} + \boldsymbol{C}_1^{-} & \boldsymbol{0} \\ \boldsymbol{U}_1^{+} & \boldsymbol{0} & \boldsymbol{K}_1^{+} + \boldsymbol{C}_1^{+} \end{pmatrix} \tag{15}$$

with $\boldsymbol{C}_1^{-} = \boldsymbol{0}$, $\boldsymbol{C}_1^{+} = \boldsymbol{0}$, $\boldsymbol{U}_1^{-} = \boldsymbol{U}_1^{-,(1)}$, and $\boldsymbol{U}_1^{+} = \boldsymbol{U}_1^{+,(1)}$. Here, $\boldsymbol{f}$ represents the Fock matrix in the orbital basis.

The resulting ADC-*GW* Hamiltonian corresponds to the standard *GW* self-energy in its upfolded form.[27,121−126] In other words, the associated ADC-*GW* scheme is formally equivalent to the conventional *GW* approximation. In this case, the ADC procedure does not introduce any additional terms, which is expected since the *GW* self-energy already admits a spectral representation.[83] This situation is closely analogous to the equivalence between ADC(2) and the second-order Green's function (GF2) self-energy.[117]

Going beyond the *GW* approximation, one may apply the ADC procedure to the first three terms of $\boldsymbol{\Sigma}^{\pm}$. These terms form the 2SOSEX-aug self-energy introduced in ref 83. and defined as the 2SOSEX self-energy [see eq 4] with one additional second-order exchange term of the form $\mathrm{i}^2 G\nu G\nu G$. This leads to additional contributions to the coupling blocks

$$(\boldsymbol{U}_1^{-,(2)})_{i\nu,q} = \sum_{kc}\frac{M^{*}_{ck,\nu}\langle ic|kq\rangle}{\epsilon_c - \epsilon_k + \Omega_\nu} + \sum_{kc}\frac{M^{*}_{kc,\nu}\langle ik|cq\rangle}{\epsilon_c - \epsilon_k - \Omega_\nu} \tag{16a}$$

https://doi.org/10.1021/acs.jpclett.6c01904
J. Phys. Chem. Lett. 2026, 17, 8541−8551

Table 1. Composition of the Various Blocks Entering the Different ADC-Based Schemes Considered in This Work[a]

Blocks	Config.	ADC-*GW*	ADC-2SOSEX	ADC(3)-*G*3*W*2	ADC-*G*3*W*2
$\boldsymbol{U}_1^-$	2h1p	$\boldsymbol{U}_1^{-,(1)}$	$\boldsymbol{U}_1^{-,(1)} + \boldsymbol{U}_1^{-,(2)}$	$\boldsymbol{U}_1^{-,(1)} + \boldsymbol{U}_1^{-,(2)}$	$\boldsymbol{U}_1^{-,(1)} + \boldsymbol{U}_1^{-,(3)}$
$\boldsymbol{U}_1^+$	2p1h	$\boldsymbol{U}_1^{+,(1)}$	$\boldsymbol{U}_1^{+,(1)} + \boldsymbol{U}_1^{+,(2)}$	$\boldsymbol{U}_1^{+,(1)} + \boldsymbol{U}_1^{+,(2)}$	$\boldsymbol{U}_1^{+,(1)} + \boldsymbol{U}_1^{+,(2)} + \boldsymbol{U}_1^{+,(3)}$
$\boldsymbol{K}_1^- + \boldsymbol{C}_1^-$	2h1p	$\boldsymbol{K}_1^-$	$\boldsymbol{K}_1^-$	$\boldsymbol{K}_1^- + \boldsymbol{C}_1^{-,(1)}$	$\boldsymbol{K}_1^- + \boldsymbol{C}_1^{-,(1)}$
$\boldsymbol{K}_1^+ + \boldsymbol{C}_1^+$	2p1h	$\boldsymbol{K}_1^+$	$\boldsymbol{K}_1^+$	$\boldsymbol{K}_1^+ + \boldsymbol{C}_1^{+,(1)}$	$\boldsymbol{K}_1^+ + \boldsymbol{C}_1^{+,(1)}$
$\boldsymbol{U}_2^-$	3h2p	**0**	**0**	**0**	$\boldsymbol{U}_2^{-,(1)}$
$\boldsymbol{U}_2^+$	3p2h	**0**	**0**	**0**	$\boldsymbol{U}_2^{+,(1)}$
$\boldsymbol{K}_2^- + \boldsymbol{C}_2^-$	3h2p	**0**	**0**	**0**	$\boldsymbol{K}_2^-$
$\boldsymbol{K}_2^+ + \boldsymbol{C}_2^+$	3p2h	**0**	**0**	**0**	$\boldsymbol{K}_2^+$
$\boldsymbol{C}_{1/2}^-$	2h1p/3h2p	**0**	**0**	**0**	$\boldsymbol{C}_{1/2}^{-,(1)}$
$\boldsymbol{C}_{1/2}^+$	2p1h/3p2h	**0**	**0**	**0**	$\boldsymbol{C}_{1/2}^{+,(1)}$

[a]See the main text for the explicit expression of each block.

$$(\boldsymbol{U}_1^{+,(2)})_{a\nu,q} = \sum_{kc} \frac{M_{ck,\nu}\langle ak|cq\rangle}{\epsilon_c - \epsilon_k + \Omega_\nu} + \sum_{kc} \frac{M_{kc,\nu}\langle ac|kq\rangle}{\epsilon_c - \epsilon_k - \Omega_\nu} \tag{16b}$$

that must be included in the effective Hamiltonian [see eq 15]. The ADC scheme with all contributions determined so far is referred to as ADC-2SOSEX. The composition of the various blocks entering the effective Hamiltonian in the different ADC-based schemes considered here is summarized in Table 1.

When including the corresponding contributions in eq 8, one can see that the ADC-2SOSEX self-energy has two additional terms, $[\boldsymbol{U}_1^{-,(2)}]^\dagger\cdot(\boldsymbol{\omega} - \boldsymbol{K}_1^-)^{-1}\cdot\boldsymbol{U}_1^{-,(2)}$ and $[\boldsymbol{U}_1^{+,(2)}]^\dagger\cdot(\boldsymbol{\omega} - \boldsymbol{K}_1^+)^{-1}\cdot\boldsymbol{U}_1^{+,(2)}$, compared to the 2SOSEX-aug self-energy. In this case, the ADC procedure generates only a finite number of additional contributions because there are no contributions in the $\boldsymbol{C}^\pm$ blocks so far [see eq 10]. Note that ADC-2SOSEX is exactly equivalent to the *GW*+2SOSEX-psd self-energy reported in ref 83. and derived using the procedure of refs 112−114.

Proceeding toward the full *G*3*W*2 self-energy, the next contributions to be included correspond to the fourth term in eq 11, which determines the first contribution to the diagonal blocks

$$(\boldsymbol{C}_1^{-,(1)})_{i\nu,j\mu} = \frac{1}{2}\sum_c \frac{M_{ic,\mu}M_{jc,\nu}^*}{\epsilon_i - \epsilon_c + \Omega_\mu} + \frac{1}{2}\sum_c \frac{M_{ic,\mu}M_{jc,\nu}^*}{\epsilon_j - \epsilon_c + \Omega_\nu} \tag{17a}$$

$$(\boldsymbol{C}_1^{+,(1)})_{a\nu,b\mu} = \frac{1}{2}\sum_k \frac{M_{ka,\mu}^*M_{kb,\nu}}{\epsilon_a - \epsilon_k - \Omega_\mu} + \frac{1}{2}\sum_k \frac{M_{ka,\mu}^*M_{kb,\nu}}{\epsilon_b - \epsilon_k - \Omega_\nu} \tag{17b}$$

The ADC scheme incorporating all contributions identified thus far will be referred to as ADC(3)-*G*3*W*2 (see Table 1). At this stage, the inclusion of $\boldsymbol{C}$ in the resolvent $(\boldsymbol{\omega} - \boldsymbol{K} - \boldsymbol{C})^{-1}$ effectively generates an infinite resummation of diagrams.

Finally, applying the ADC procedure to the full *G*3*W*2 self-energy [see eq 11] yields a new approximation to the self-energy, which we denote ADC-*G*3*W*2. The remaining *G*3*W*2 self-energy terms not yet accounted for provide a third contribution to the coupling blocks

$$\begin{aligned}(\boldsymbol{U}_1^{-,(3)})_{i\nu,q} = {} & \frac{1}{2}\sum_{kc\mu} \frac{M_{ic,\mu}M_{kc,\nu}^*M_{qk,\mu}^*}{(\epsilon_c - \epsilon_k - \Omega_\nu)(\epsilon_c - \epsilon_i - \Omega_\mu)} \\ & - \sum_{kc\mu} \frac{M_{ci,\mu}^*M_{kc,\nu}^*M_{kq,\mu}}{(\epsilon_c - \epsilon_k - \Omega_\nu)(\epsilon_c - \epsilon_i + \Omega_\mu)} \\ & - \sum_{kc\mu} \frac{M_{ki,\mu}^*M_{ck,\nu}^*M_{cq,\mu}}{(\epsilon_c - \epsilon_i + \Omega_\nu + \Omega_\mu)(\epsilon_c - \epsilon_k + \Omega_\nu)} \\ & + \sum_{cd\mu} \frac{M_{di,\mu}^*M_{cd,\nu}^*M_{cq,\mu}}{(\epsilon_c - \epsilon_i + \Omega_\nu + \Omega_\mu)(\epsilon_d - \epsilon_i + \Omega_\mu)}\end{aligned} \tag{18a}$$

$$\begin{aligned}(\boldsymbol{U}_1^{+,(3)})_{a\nu,q} = {} & \frac{1}{2}\sum_{kc\mu} \frac{M_{ka,\mu}^*M_{kc,\nu}M_{cq,\mu}}{(\epsilon_c - \epsilon_k - \Omega_\nu)(\epsilon_a - \epsilon_k - \Omega_\mu)} \\ & - \sum_{kc\mu} \frac{M_{ak,\mu}M_{kc,\nu}M_{qc,\mu}^*}{(\epsilon_c - \epsilon_k - \Omega_\nu)(\epsilon_a - \epsilon_k + \Omega_\mu)} \\ & - \sum_{kc\mu} \frac{M_{ac,\mu}M_{ck,\nu}M_{qk,\mu}^*}{(\epsilon_a - \epsilon_k + \Omega_\nu + \Omega_\mu)(\epsilon_c - \epsilon_k + \Omega_\nu)} \\ & + \sum_{kl\mu} \frac{M_{al,\mu}M_{lk,\nu}M_{qk,\mu}^*}{(\epsilon_a - \epsilon_k + \Omega_\nu + \Omega_\mu)(\epsilon_a - \epsilon_l + \Omega_\mu)}\end{aligned} \tag{18b}$$

They also introduce additional diagonal blocks corresponding to the inclusion of three-hole-two-particle (3h2p) and three-particle-two-hole (3p2h) configurations

$$(\boldsymbol{K}_2^-)_{i\nu\mu,j\lambda\sigma} = (\epsilon_i - \Omega_\nu - \Omega_\mu)\delta_{ij}\delta_{\nu\lambda}\delta_{\mu\sigma} \tag{19a}$$

$$(\boldsymbol{K}_2^+)_{a\nu\mu,b\lambda\sigma} = (\epsilon_a + \Omega_\nu + \Omega_\mu)\delta_{ab}\delta_{\nu\lambda}\delta_{\mu\sigma} \tag{19b}$$

together with the corresponding coupling blocks

$$(\boldsymbol{U}_2^{-,(1)})_{i\nu\mu,q} = -\sum_c \frac{M_{ci,\mu}^*M_{qc,\nu}^*}{\epsilon_c - \epsilon_i + \Omega_\mu} \tag{20a}$$

$$(\boldsymbol{U}_2^{+,(1)})_{a\nu\mu,q} = +\sum_k \frac{M_{ak,\mu}M_{kq,\nu}}{\epsilon_a - \epsilon_k + \Omega_\mu} \tag{20b}$$

Finally, couplings arise between the 2h1p and 3h2p configurations, as well as between the 2p1h and 3p2h configurations

https://doi.org/10.1021/acs.jpclett.6c01904
J. Phys. Chem. Lett. 2026, 17, 8541−8551

$$(\boldsymbol{C}^{-,(1)}_{2/1})_{i\nu\mu,j\lambda} = M^{*}_{ji,\mu}\delta_{\nu\lambda} \tag{21a}$$

$$(\boldsymbol{C}^{+,(1)}_{2/1})_{a\nu\mu,b\lambda} = M_{ab,\mu}\delta_{\nu\lambda} \tag{21b}$$

As a result, the effective Hamiltonian must be expanded to include the 3h2p and 3p2h configurations with respect to eq 15, leading to

$$\boldsymbol{H} = \begin{pmatrix} \boldsymbol{f} & (\boldsymbol{U}^{-}_{1})^{\dagger} & (\boldsymbol{U}^{-}_{2})^{\dagger} & (\boldsymbol{U}^{+}_{1})^{\dagger} & (\boldsymbol{U}^{+}_{2})^{\dagger} \\ \boldsymbol{U}^{-}_{1} & \boldsymbol{K}^{-}_{1} + \boldsymbol{C}^{-}_{1} & (\boldsymbol{C}^{-}_{2/1})^{\dagger} & \boldsymbol{0} & \boldsymbol{0} \\ \boldsymbol{U}^{-}_{2} & \boldsymbol{C}^{-}_{2/1} & \boldsymbol{K}^{-}_{2} + \boldsymbol{C}^{-}_{2} & \boldsymbol{0} & \boldsymbol{0} \\ \boldsymbol{U}^{+}_{1} & \boldsymbol{0} & \boldsymbol{0} & \boldsymbol{K}^{+}_{1} + \boldsymbol{C}^{+}_{1} & (\boldsymbol{C}^{+}_{2/1})^{\dagger} \\ \boldsymbol{U}^{+}_{2} & \boldsymbol{0} & \boldsymbol{0} & \boldsymbol{C}^{+}_{2/1} & \boldsymbol{K}^{+}_{2} + \boldsymbol{C}^{+}_{2} \end{pmatrix} \tag{22}$$

Starting from eq 11, ADC-*G*3*W*2 thus performs an infinite resummation of diagrams, yielding an approximation that admits a spectral representation.

As can be seen from the above equation, the effective Hamiltonian associated with this ADC-based resummation is Hermitian. This property follows from the particular expression of the self-energy [see Eq. 11] used to derive the various blocks. Specifically, this expression was obtained following the procedure introduced in ref 83., where the authors showed that decomposing dressed poles of the form $\omega - \epsilon_p \pm \Omega_\nu$ together with bare poles (i.e., involving three single-particle energies) in the *G*3*W*2 self-energy yields a self-energy expressed solely in terms of dressed poles. The ADC procedure could, in principle, have been applied directly to the *G*3*W*2 self-energy prior to this decomposition. However, the resulting resummation would then be associated with a non-Hermitian effective Hamiltonian. Although the decomposition strategy can, in principle, be extended to any vertex correction to the self-energy, there is no guarantee that a form yielding a Hermitian effective Hamiltonian can always be found. Finally, it is worth noting that the resummation performed prior to pole decomposition can be described using the standard Goldstone diagrammatic rules. By contrast, the terms appearing in Eq. 11 after decomposition cannot be represented within this framework.

Multiple implementations of the various schemes have been benchmarked using two complementary approaches: either full diagonalization of the resulting Hermitian matrices, performed with the QUACK software,[127] or a root-following Davidson algorithm implemented in a Python code that heavily relies on functionalities provided by PySCF.[128,129] The computational scaling of the Davidson-based implementation for the determination of a single root is reported in Table 2, together with an example of a contraction/intermediate illustrating the associated computational complexity. Note that the diagonalization of the RPA eigenvalue problem, which scales as $O(K^6)$ (K being the number of basis functions), and the integral transformation, which scales as $O(K^5)$, required to construct $M_{pq,\nu}$ are not included in these estimates, as they are common to all methods.

In all calculations, Hartree−Fock orbitals and energies are used as a starting point, the broadening parameter η is set to zero, and the Davidson solver used to compute the quasiparticle energies is converged to a threshold of 10^{-8} E_h.

Table 2. Computational Scaling of the Various ADC Schemes Presented in This Work, Together with an Example of Contraction/Intermediate Illustrating the Origin of Their Overall Scaling[a]

Method	Scaling	Contraction/Intermediate
ADC-*GW*	$O(K^4)$	$\sum_{bv} M_{ab,v} r^{(n)}_{bv}$
ADC-2SOSEX	$O(K^5)$	$\sum_{v} \frac{M_{ck,v}}{\epsilon_c - \epsilon_k + \Omega_v} r^{(n)}_{bv}$
ADC(3)-*G*3*W*2	$O(K^5)$	$\sum_{v} \frac{M_{ck,v}}{\epsilon_c - \epsilon_k + \Omega_v} r^{(n)}_{bv}$
ADC-*G*3*W*2	$O(K^7)$	$\frac{M^{*}_{di,\mu}}{(\epsilon_c - \epsilon_i + \Omega_v + \Omega_\mu)(\epsilon_d - \epsilon_i + \Omega_\mu)}$

[a]The diagonalization of the RPA eigenvalue problem [$O(K^6)$] and the integral transformation [$O(K^5)$] required to construct $M_{pq,\nu}$ [see Eq. 12] are common to all methods and are therefore not included in these estimates. Here, K denotes the number of basis functions and $r^{(n)}_{bv}$ an element of the nth excitation vector.

To avoid numerical instabilities associated with small energy denominators, we employ an energy-dependent regularization scheme with the flow parameter fixed at $s = 10^6$.[126,130] This large value of s corresponds to an extremely weak regularization, effectively leading to unregularized results. The 2SOSEX and *G*3*W*2 calculations have been performed with QUACK and the implementation has been verified against MOLGW.[131] The corresponding quasiparticle energies have been obtained by solving the frequency-dependent quasiparticle equation within the diagonal approximation, i.e., for each orbital independently. Moreover, we have implemented the Dyson version of ADC(2) and ADC(3) in their spin-adapted form.[116,132] Non-Dyson ADC(2) and ADC(3)[133−137] calculations have been performed with PySCF.[128,129]

Here, we consider the set of inner- and outer-valence IPs designed in ref 28., which is composed of 58 valence IPs computed in small molecular systems. The molecular geometries have been extracted from the same study. The reference IPs, the so-called theoretical best estimates (TBEs), are computed at the full configuration interaction (FCI) level and are thus highly accurate. All IPs are computed in the aug-cc-pVDZ basis set.

First, we compute this set of IPs within the diagonal approximation using the following methods: ADC-*GW* (equivalent to the one-shot G_0W_0 scheme), 2SOSEX, ADC-2SOSEX (equivalent to 2SOSEX-psd[83]), *G*3*W*2, and ADC-*G*3*W*2. The diagonal approximation in ADC schemes corresponds to restricting the Fock matrix to a single orbital energy and diagonalizing it for each orbital. We then consider several ADC schemes, namely ADC-*GW*, ADC-2SOSEX, ADC(3)-*G*3*W*2, and ADC-*G*3*W*2, beyond the diagonal approximation, i.e., the effective Hamiltonian is diagonalized once, and all quasiparticle energies are obtained from a single calculation. All the raw data can be found in the Supporting Information. In addition, we evaluate the same set of IPs at the ADC(2) and ADC(3) levels within the Dyson formalism. In this framework, the hole and electron sectors are coupled, as in the ADC schemes developed in the present study. For completeness, the Supporting Information also reports the corresponding non-Dyson ADC(2) and ADC(3) results, in which the two sectors are decoupled. These results show that, while Dyson and non-Dyson ADC(2) yield similar IPs, the differences become significantly more pronounced at the ADC(3) level (see below).[138−140]

https://doi.org/10.1021/acs.jpclett.6c01904
J. Phys. Chem. Lett. 2026, 17, 8541−8551

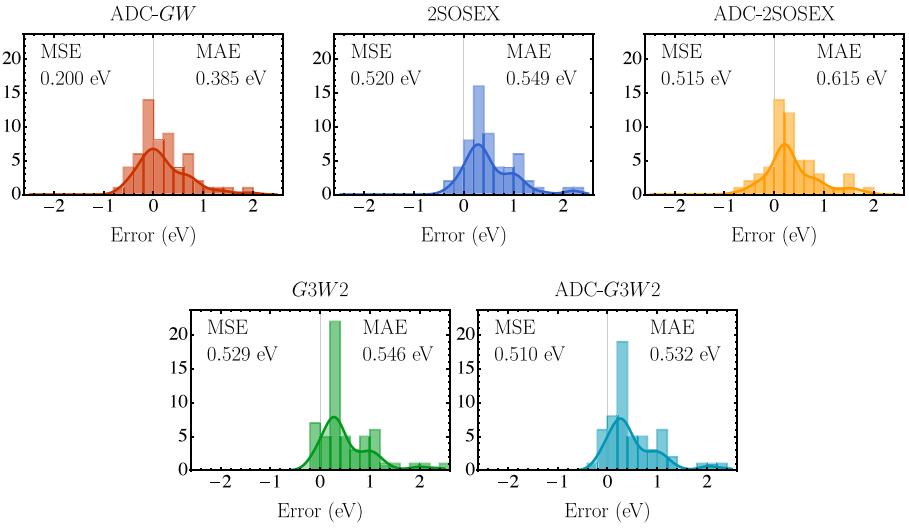

Figure 2. Histogram of the errors (with respect to the TBEs) for the inner- and outer-valence IPs computed with various self-energy schemes in the aug-cc-pVDZ basis set. All calculations are performed in the diagonal approximation.

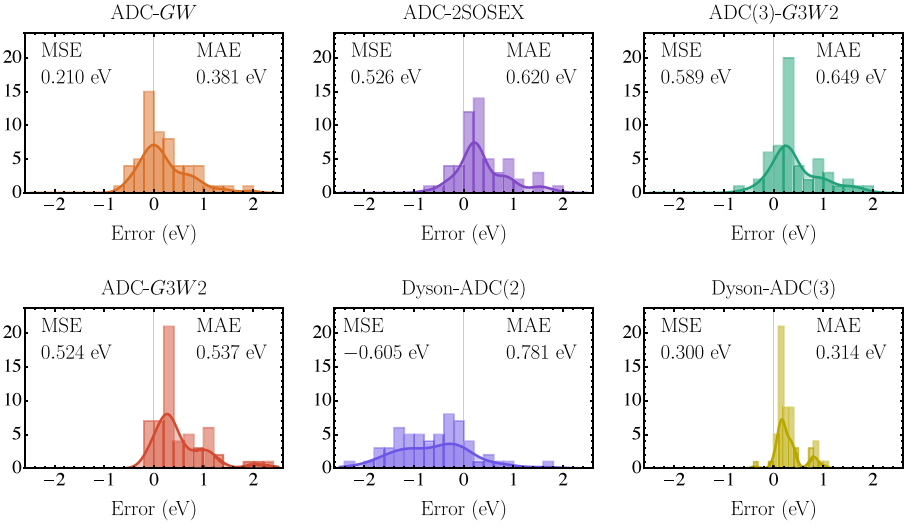

Figure 3. Histogram of the errors (with respect to the TBEs) for the inner- and outer-valence IPs computed with various ADC schemes in the aug-cc-pVDZ basis set. All calculations are performed without diagonal approximation.

Figure 2 reports the error distribution (with respect to the TBEs) for the various self-energies within the diagonal approximation. The *GW* approximation yields a MAE of 0.385 eV and a MSE of 0.200 eV, in agreement with previous reports for this set of IPs.[28,141] The 2SOSEX and ADC-2SOSEX approximations yield similar MSEs (0.520 and 0.515 eV, respectively), while the MAE of ADC-2SOSEX (0.615 eV) is slightly larger than that of its 2SOSEX counterpart (0.559 eV). This trend contrasts with the findings of ref 83, where Bruneval and co-workers reported that, using the same set of Hartree−Fock starting orbitals, the 2SOSEX-psd self-energy provides more accurate results than 2SOSEX for the *GW*100 benchmark set (MAEs of 0.29 and 0.49 eV, respectively). It is worth noting that *GW*100 contains only principal IPs, whereas the present set additionally includes inner-valence excitations, which are significantly more challenging to describe, even at the *GW* level. Finally, *G*3*W*2 yields a MAE of 0.546 eV and a MSE of 0.529 eV, in line with results obtained for the *GW*100 benchmark, where a MAE of 0.51 eV was reported.[82] Within the diagonal approximation, ADC-G3W2 yields a MAE of 0.532 eV and a MSE of 0.510 eV, slightly improving these statistical indicators without substantially altering the overall picture.

In Figure 3, we report the error distribution (with respect to the TBEs) for the various ADC schemes. Among these, ADC-*GW* yields the smallest MAE of 0.381 eV. This MAE increases to 0.620 eV for ADC-2SOSEX and further to 0.649 eV for ADC(3)-*G*3*W*2, before decreasing to 0.537 eV for ADC-*G*3*W*2. A similar trend is observed for the MSEs, which are all positive and of comparable magnitude to the corresponding MAEs (see Figure 3). For comparison, ADC(2) and ADC(3) yield MAEs of 0.781 and 0.314 eV, respectively, with MSEs of opposite sign [−0.605 eV for ADC(2) and 0.300 eV for ADC(3)]. For the corresponding non-Dyson variants, the MAEs are 0.851 eV for ADC(2) and 0.404 eV for ADC(3), while the MSEs amount to − 0.683 and 0.293 eV, respectively (see the Supporting Information). As mentioned earlier, decoupling the hole and electron sectors has little effect on the IPs at the ADC(2) level, whereas it noticeably increases the MAE at the ADC(3) level. As anticipated, ADC-*G*3*W*2 is

https://doi.org/10.1021/acs.jpclett.6c01904
J. Phys. Chem. Lett. 2026, 17, 8541−8551

found to be less accurate than the conventional ADC-*GW* scheme. Nevertheless, the inclusion of inner-vertex corrections is expected to improve the performance of ADC-*G*3*W*2, while the accuracy of ADC-*GW* is known to deteriorate as the description of screening is refined.[25,106,108] We hope to report on such inner-vertex corrections within ADC-*G*3*W*2 in future work.

The present work may be viewed as an ADC-based treatment of outer-vertex corrections to the self-energy, thereby providing a beyond-*GW* self-energy that retains the correct spectral representation. A natural and important next step is therefore to identify the corresponding inner-vertex corrections that should accompany this approach, in order to restore consistency between the self-energy and the polarizability. Such a balanced treatment is expected to improve the accuracy of the method.

From a practical perspective, non-Dyson variants of the ADC-*G*3*W*2 schemes appear attractive, as they avoid the need for a root-following Davidson algorithm.[133−137] While non-Dyson approaches have been explored at the *GW* level,[121,124,141] their behavior within the *G*3*W*2 framework remains largely unexplored and therefore warrants systematic investigation. In addition, another natural perspective for this work would be to perform these calculations self-consistently, or include an effective static contribution to the self-energy, which could be used to mimic partial self-consistency effects. Although such static corrections have been formulated at the *GW* level,[142−144] their extension to the *G*3*W*2 approximation remains to be derived.

Beyond these developments, extending the present ADC-based *GW* and *G*3*W*2 schemes to the multireference case constitutes another appealing yet challenging direction for future work. Multireference extensions within the ADC framework have recently been proposed.[140,145−149] Although encouraging results have been reported recently,[67] the most suitable strategy for incorporating multireference effects into the present formalism remains unclear at this stage. Together, these perspectives outline several promising avenues for extending the present framework toward a more complete, accurate, and efficient description of electronic correlation within many-body perturbation theory.

Finally, it is worth noting that ADC and coupled-cluster theories[150−154] share a common diagrammatic language rooted in Goldstone diagrams, which has already enabled the establishment of formal connections between these approaches.[139,155−159] In this context, the present links between ADC and *GW* may contribute to a deeper understanding of the relationships between many-body perturbation theory and coupled-cluster methodologies. Recent studies have further clarified these connections, revealing deep formal links and offering a unified perspective on the respective strengths and limitations of these frameworks.[123,124,160−167]

■ ASSOCIATED CONTENT

Supporting Information

The Supporting Information is available free of charge at https://pubs.acs.org/doi/10.1021/acs.jpclett.6c01904.

Derivation of the *G*3*W*2 self-energy and of the ADC-*G*3*W*2 matrix elements and raw data corresponding to the results of the main manuscript. Additional non-Dyson ADC(2) and ADC(3) results (PDF)

■ AUTHOR INFORMATION

Corresponding Authors

Antoine Marie − *Laboratoire de Chimie et Physique Quantiques (UMR 5626), Université de Toulouse, CNRS, Toulouse 31062, France;* orcid.org/0000-0003-3605-0176; Email: amarie@irsamc.ups-tlse.fr

Johannes Tölle − *Department of Chemistry and The Hamburg Centre for Ultrafast Imaging (CUI), University of Hamburg, 22761 Hamburg, Germany;* orcid.org/0000-0002-2414-7758; Email: johannes.toelle@uni-hamburg.de

Pierre-François Loos − *Laboratoire de Chimie et Physique Quantiques (UMR 5626), Université de Toulouse, CNRS, Toulouse 31062, France;* orcid.org/0000-0003-0598-7425; Email: loos@irsamc.ups-tlse.fr

Complete contact information is available at: https://pubs.acs.org/10.1021/acs.jpclett.6c01904

Notes

The authors declare no competing financial interest.

■ ACKNOWLEDGMENTS

This project has received funding from the European Research Council (ERC) under the European Union's Horizon 2020 research and innovation programme (Grant agreement No. 863481). J.T. acknowledges funding from the Fonds der Chemischen Industrie (FCI) via a Liebig fellowship and support by the Cluster of Excellence "CUI: Advanced Imaging of Matter" of the Deutsche Forschungsgemeinschaft (DFG) (EXC 2056, funding ID 390715994). J.T. also acknowledges financial support by the Emmy Noether Program of the German Research Foundation (project number 577598009). This work used the HPC resources from CALMIP (Toulouse) under allocation 2026-18005.

■ REFERENCES

(1) Onida, G.; Reining, L.; Rubio, A. Electronic Excitations: Density-Functional Versus Many-Body Green's Function Approaches. *Rev. Mod. Phys.* **2002**, *74*, 601−659.

(2) Martin, R. M.; Reining, L.; Ceperley, D. M. *Interacting Electrons: Theory and Computational Approaches*; Cambridge University Press: 2016.

(3) Reining, L. The *GW* Approximation: Content, Successes and Limitations: The *GW* Approximation. *Wiley Interdiscip. Rev. Comput. Mol. Sci.* **2018**, *8*, No. e1344.

(4) Golze, D.; Dvorak, M.; Rinke, P. The *GW* Compendium: A Practical Guide to Theoretical Photoemission Spectroscopy. *Front. Chem.* **2019**, *7*, 377.

(5) Marie, A.; Ammar, A.; Loos, P.-F. The GW approximation: A quantum chemistry perspective. *Adv. Quantum Chem.* **2024**, *90*, 157−184.

(6) Blase, X.; Duchemin, I.; Jacquemin, D. The Bethe−Salpeter equation in chemistry: relations with TD-DFT, applications and challenges. *Chem. Soc. Rev.* **2018**, *47*, 1022−1043.

(7) Blase, X.; Duchemin, I.; Jacquemin, D.; Loos, P.-F. The Bethe−Salpeter Equation Formalism: From Physics to Chemistry. *J. Phys. Chem. Lett.* **2020**, *11*, 7371−7382.

(8) Strinati, G.; Mattausch, H. J.; Hanke, W. Dynamical Aspects of Correlation Corrections in a Covalent Crystal. *Phys. Rev. B* **1982**, *25*, 2867−2888.

(9) Strinati, G. Dynamical Shift and Broadening of Core Excitons in Semiconductors. *Phys. Rev. Lett.* **1982**, *49*, 1519.

(10) Hybertsen, M. S.; Louie, S. G. First-Principles Theory of Quasiparticles: Calculation of Band Gaps in Semiconductors and Insulators. *Phys. Rev. Lett.* **1985**, *55*, 1418−1421.

(11) Hybertsen, M. S.; Louie, S. G. Electron Correlation in Semiconductors and Insulators: Band Gaps and Quasiparticle Energies. *Phys. Rev. B* **1986**, *34*, 5390−5413.
(12) Godby, R. W.; Schlüter, M.; Sham, L. J. Accurate Exchange-Correlation Potential for Silicon and Its Discontinuity on Addition of an Electron. *Phys. Rev. Lett.* **1986**, *56*, 2415−2418.
(13) Godby, R. W.; Schlüter, M.; Sham, L. J. Quasiparticle Energies in GaAs and AlAs. *Phys. Rev. B* **1987**, *35*, 4170−4171.
(14) Shirley, E. L.; Martin, R. M. *GW* quasiparticle calculations in atoms. *Phys. Rev. B* **1993**, *47*, 15404−15412.
(15) Rohlfing, M.; Louie, S. G. Electron-hole excitations and optical spectra from first principles. *Phys. Rev. B* **2000**, *62*, 4927−4944.
(16) Stan, A.; Dahlen, N. E.; van Leeuwen, R. Fully Self-Consistent *GW* Calculations for Atoms and Molecules. *Europhys. Lett.* **2006**, *76*, 298−304.
(17) Rostgaard, C.; Jacobsen, K. W.; Thygesen, K. S. Fully Self-Consistent *GW* Calculations for Molecules. *Phys. Rev. B* **2010**, *81*, No. 085103.
(18) Blase, X.; Attaccalite, C.; Olevano, V. First-Principles *GW* Calculations for Fullerenes, Porphyrins, Phtalocyanine, and Other Molecules of Interest for Organic Photovoltaic Applications. *Phys. Rev. B* **2011**, *83*, No. 115103.
(19) Faber, C.; Attaccalite, C.; Olevano, V.; Runge, E.; Blase, X. First-Principles *GW* Calculations for DNA and RNA Nucleobases. *Phys. Rev. B* **2011**, *83*, No. 115123.
(20) Ke, S.-H. All-Electron *GW* Methods Implemented in Molecular Orbital Space: Ionization Energy and Electron Affinity of Conjugated Molecules. *Phys. Rev. B* **2011**, *84*, No. 205415.
(21) Bruneval, F. Ionization Energy of Atoms Obtained from *GW* Self-Energy or from Random Phase Approximation Total Energies. *J. Chem. Phys.* **2012**, *136*, No. 194107.
(22) Bruneval, F.; Marques, M. A. L. Benchmarking the Starting Points of the *GW* Approximation for Molecules. *J. Chem. Theory Comput.* **2013**, *9*, 324−329.
(23) van Setten, M. J.; Caruso, F.; Sharifzadeh, S.; Ren, X.; Scheffler, M.; Liu, F.; Lischner, J.; Lin, L.; Deslippe, J. R.; Louie, S. G.; Yang, C.; Weigend, F.; Neaton, J. B.; Evers, F.; Rinke, P. *GW*100: Benchmarking G_0W_0 for Molecular Systems. *J. Chem. Theory Comput.* **2015**, *11*, 5665−5687.
(24) Caruso, F.; Dauth, M.; van Setten, M. J.; Rinke, P. Benchmark of *GW* Approaches for the *GW*100 Test Set. *J. Chem. Theory Comput.* **2016**, *12*, 5076.
(25) Lewis, A. M.; Berkelbach, T. C. Vertex Corrections to the Polarizability Do Not Improve the *GW* Approximation for the Ionization Potential of Molecules. *J. Chem. Theory Comput.* **2019**, *15*, 2925.
(26) Bruneval, F.; Dattani, N.; van Setten, M. J. The *GW* Miracle in Many-Body Perturbation Theory for the Ionization Potential of Molecules. *Front. Chem.* **2021**, *9*, No. 749779.
(27) Monino, E.; Loos, P.-F. Connections and performances of Green's function methods for charged and neutral excitations. *J. Chem. Phys.* **2023**, *159*, No. 034105.
(28) Marie, A.; Loos, P.-F. Reference Energies for Valence Ionizations and Satellite Transitions. *J. Chem. Theory Comput.* **2024**, *20*, 4751−4777.
(29) van Setten, M. J.; Costa, R.; Viñes, F.; Illas, F. Assessing *GW* Approaches for Predicting Core Level Binding Energies. *J. Chem. Theory Comput.* **2018**, *14*, 877−883.
(30) Golze, D.; Wilhelm, J.; van Setten, M. J.; Rinke, P. Core-Level Binding Energies from *GW*: An Efficient Full-Frequency Approach within a Localized Basis. *J. Chem. Theory Comput.* **2018**, *14*, 4856−4869.
(31) Golze, D.; Keller, L.; Rinke, P. Accurate Absolute and Relative Core-Level Binding Energies from *GW*. *J. Phys. Chem. Lett.* **2020**, *11*, 1840−1847.
(32) Mejia-Rodriguez, D.; Kunitsa, A.; Aprà, E.; Govind, N. Scalable Molecular *GW* Calculations: Valence and Core Spectra. *J. Chem. Theory Comput.* **2021**, *17*, 7504−7517.
(33) Li, J.; Jin, Y.; Rinke, P.; Yang, W.; Golze, D. Benchmark of *GW* Methods for Core-Level Binding Energies. *J. Chem. Theory Comput.* **2022**, *18*, 7570−7585.
(34) Mukatayev, I.; Moevus, F.; Sklénard, B.; Olevano, V.; Li, J. XPS Core-Level Chemical Shift by Ab Initio Many-Body Theory. *J. Phys. Chem. A* **2023**, *127*, 1642−1648.
(35) Panadés-Barrueta, R. L.; Golze, D. Accelerating Core-Level *GW* Calculations by Combining the Contour Deformation Approach with the Analytic Continuation of *W*. *J. Chem. Theory Comput.* **2023**, *19*, 5450−5464.
(36) Grossman, J. C.; Rohlfing, M.; Mitas, L.; Louie, S. G.; Cohen, M. L. High Accuracy Many-Body Calculational Approaches for Excitations in Molecules. *Phys. Rev. Lett.* **2001**, *86*, 472−475.
(37) Tiago, M. L.; Chelikowsky, J. R. Optical Excitations in Organic Molecules, Clusters, and Defects Studied by First-Principles Green's Function Methods. *Phys. Rev. B* **2006**, *73*, No. 205334.
(38) Rocca, D.; Lu, D.; Galli, G. Ab Initio Calculations of Optical Absorption Spectra: Solution of the Bethe−Salpeter Equation Within Density Matrix Perturbation Theory. *J. Chem. Phys.* **2010**, *133*, No. 164109.
(39) Blase, X.; Attaccalite, C. Charge-Transfer Excitations in Molecular Donor-Acceptor Complexes within the Many-Body Bethe-Salpeter Approach. *Appl. Phys. Lett.* **2011**, *99*, No. 171909.
(40) Baumeier, B.; Andrienko, D.; Rohlfing, M. Frenkel and Charge-Transfer Excitations in Donor−Acceptor Complexes From Many-Body Green's Functions Theory. *J. Chem. Theory Comput.* **2012**, *8*, 2790−2795.
(41) Duchemin, I.; Deutsch, T.; Blase, X. Short-Range to Long-Range Charge-Transfer Excitations in the Zincbacteriochlorin-Bacteriochlorin Complex: A Bethe-Salpeter Study. *Phys. Rev. Lett.* **2012**, *109*, No. 167801.
(42) Bruneval, F.; Hamed, S. M.; Neaton, J. B. A systematic benchmark of the ab initio Bethe-Salpeter equation approach for low-lying optical excitations of small organic molecules. *J. Chem. Phys.* **2015**, *142*, No. 244101.
(43) Leng, X.; Jin, F.; Wei, M.; Ma, Y. *GW* Method and Bethe-Salpeter Equation for Calculating Electronic Excitations: *GW* Method and Bethe-Salpeter Equation. *Wiley Interdiscip. Rev. Comput. Mol. Sci.* **2016**, *6*, 532−550.
(44) Hirose, D.; Noguchi, Y.; Sugino, O. All-Electron *GW*+Bethe-Salpeter Calculations on Small Molecules. *Phys. Rev. B* **2015**, *91*, No. 205111.
(45) Jacquemin, D.; Duchemin, I.; Blase, X. Is the Bethe−Salpeter Formalism Accurate for Excitation Energies? Comparisons with TD-DFT, CASPT2, and EOM-CCSD. *J. Phys. Chem. Lett.* **2017**, *8*, 1524−1529.
(46) Jacquemin, D.; Duchemin, I.; Blondel, A.; Blase, X. Benchmark of Bethe-Salpeter for Triplet Excited-States. *J. Chem. Theory Comput.* **2017**, *13*, 767−783.
(47) Krause, K.; Klopper, W. Implementation of the Bethe-Salpeter equation in the TURBOMOLE program. *J. Comput. Chem.* **2017**, *38*, 383−388.
(48) Liu, C.; Kloppenburg, J.; Yao, Y.; Ren, X.; Appel, H.; Kanai, Y.; Blum, V. All-electron ab initio Bethe-Salpeter equation approach to neutral excitations in molecules with numeric atom-centered orbitals. *J. Chem. Phys.* **2020**, *152*, No. 044105.
(49) McKeon, C. A.; Hamed, S. M.; Bruneval, F.; Neaton, J. B. An optimally tuned range-separated hybrid starting point for ab initio *GW* plus Bethe−Salpeter equation calculations of molecules. *J. Chem. Phys.* **2022**, *157*, No. 074103.
(50) Neuhauser, D.; Gao, Y.; Arntsen, C.; Karshenas, C.; Rabani, E.; Baer, R. Breaking the Theoretical Scaling Limit for Predicting Quasiparticle Energies: The Stochastic *GW* Approach. *Phys. Rev. Lett.* **2014**, *113*, No. 076402.
(51) Govoni, M.; Galli, G. Large Scale *GW* Calculations. *J. Chem. Theory Comput.* **2015**, *11*, 2680−2696.
(52) Vlček, V.; Rabani, E.; Neuhauser, D.; Baer, R. Stochastic *GW* Calculations for Molecules. *J. Chem. Theory Comput.* **2017**, *13*, 4997−5003.

https://doi.org/10.1021/acs.jpclett.6c01904
J. Phys. Chem. Lett. 2026, 17, 8541−8551

(53) Wilhelm, J.; Golze, D.; Talirz, L.; Hutter, J.; Pignedoli, C. A. Toward *GW* Calculations on Thousands of Atoms. *J. Phys. Chem. Lett.* **2018**, *9*, 306−312.
(54) Ben, M. D.; da Jornada, F. H.; Canning, A.; Wichmann, N.; Raman, K.; Sasanka, R.; Yang, C.; Louie, S. G.; Deslippe, J. Large-scale *GW* calculations on pre-exascale HPC systems. *Comput. Phys. Commun.* **2019**, *235*, 187−195.
(55) Förster, A.; Visscher, L. Low-Order Scaling G_0W_0 by Pair Atomic Density Fitting. *J. Chem. Theory Comput.* **2020**, *16*, 7381−7399.
(56) Kaltak, M.; Kresse, G. Minimax isometry method: A compressive sensing approach for Matsubara summation in many-body perturbation theory. *Phys. Rev. B* **2020**, *101*, No. 205145.
(57) Förster, A.; Visscher, L. Low-Order Scaling Quasiparticle Self-Consistent *GW* for Molecules. *Front. Chem.* **2021**, *9*, No. 736591.
(58) Duchemin, I.; Blase, X. Cubic-Scaling All-Electron *GW* Calculations with a Separable Density-Fitting Space−Time Approach. *J. Chem. Theory Comput.* **2021**, *17*, 2383−2393.
(59) Wilhelm, J.; Seewald, P.; Golze, D. Low-Scaling *GW* with Benchmark Accuracy and Application to Phosphorene Nanosheets. *J. Chem. Theory Comput.* **2021**, *17*, 1662−1677.
(60) Förster, A.; Visscher, L. Quasiparticle Self-Consistent *GW*-Bethe−Salpeter Equation Calculations for Large Chromophoric Systems. *J. Chem. Theory Comput.* **2022**, *18*, 6779−6793.
(61) Yu, V. W.-Z.; Govoni, M. GPU Acceleration of Large-Scale Full-Frequency *GW* Calculations. *J. Chem. Theory Comput.* **2022**, *18*, 4690−4707.
(62) Tölle, J.; Kin-Lic Chan, G. AB-G_0W_0: A practical G_0W_0 method without frequency integration based on an auxiliary boson expansion. *J. Chem. Phys.* **2024**, *160*, No. 164108.
(63) Tölle, J.; Niemeyer, N.; Neugebauer, J. Accelerating Analytic-Continuation *GW* Calculations with a Laplace Transform and Natural Auxiliary Functions. *J. Chem. Theory Comput.* **2024**, *20*, 2022−2032.
(64) Hedin, L. New Method for Calculating the One-Particle Green's Function with Application to the Electron-Gas Problem. *Phys. Rev.* **1965**, *139*, A796.
(65) Aryasetiawan, F.; Gunnarsson, O. The *GW* Method. *Rep. Prog. Phys.* **1998**, *61*, 237−312.
(66) Ammar, A.; Marie, A.; Rodríguez-Mayorga, M.; Burton, H. G. A.; Loos, P.-F. Can *GW* Handle Multireference Systems? *J. Chem. Phys.* **2024**, *160*, No. 114101.
(67) Wang, Y.; Fang, W.-H.; Li, Z. Multi-reference *GW* approximation for strongly correlated molecules. 2026; https://arxiv.org/abs/2604.16013.
(68) Verdozzi, C.; Godby, R. W.; Holloway, S. Evaluation of *GW* Approximations for the Self-Energy of a Hubbard Cluster. *Phys. Rev. Lett.* **1995**, *74*, 2327−2330.
(69) Di Sabatino, S.; Berger, J. A.; Reining, L.; Romaniello, P. Photoemission Spectra from Reduced Density Matrices: The Band Gap in Strongly Correlated Systems. *Phys. Rev. B* **2016**, *94*, No. 155141.
(70) Tomczak, J. M.; Liu, P.; Toschi, A.; Kresse, G.; Held, K. Merging *GW* with DMFT and non-local correlations beyond. *Eur. Phys. J. Spec. Top.* **2017**, *226*, 2565−2590.
(71) Dvorak, M.; Rinke, P. Dynamical configuration interaction: Quantum embedding that combines wave functions and Green's functions. *Phys. Rev. B* **2019**, *99*, No. 115134.
(72) Dvorak, M.; Golze, D.; Rinke, P. Quantum embedding theory in the screened Coulomb interaction: Combining configuration interaction with *GW*/BSE. *Phys. Rev. Mater.* **2019**, *3*, 070801.
(73) Di Sabatino, S.; Koskelo, J.; Berger, J. A.; Romaniello, P. Introducing screening in one-body density matrix functionals: Impact on charged excitations of model systems via the extended Koopmans' theorem. *Phys. Rev. B* **2022**, *105*, No. 235123.
(74) Di Sabatino, S.; Koskelo, J.; Berger, J. A.; Romaniello, P. Screened extended Koopmans' theorem: Photoemission at weak and strong correlation. *Phys. Rev. B* **2023**, *107*, No. 035111.
(75) Orlando, R.; Romaniello, P.; Loos, P.-F. The three channels of many-body perturbation theory: *GW*, particle−particle, and electron−hole *T*-matrix self-energies. *J. Chem. Phys.* **2023**, *159*, No. 184113.
(76) Mejuto-Zaera, C.; Vlček, V. c. v. Self-consistency in *GWΓ* formalism leading to quasiparticle-quasiparticle couplings. *Phys. Rev. B* **2022**, *106*, No. 165129.
(77) Loos, P.-F.; Marie, A.; Ammar, A. Cumulant Green's function methods for molecules. *Faraday Discuss.* **2024**, *254*, 240−260.
(78) Romaniello, P.; Bechstedt, F.; Reining, L. Beyond the *GW* Approximation: Combining Correlation Channels. *Phys. Rev. B* **2012**, *85*, No. 155131.
(79) Ren, X.; Marom, N.; Caruso, F.; Scheffler, M.; Rinke, P. Beyond the *GW* Approximation: A Second-Order Screened Exchange Correction. *Phys. Rev. B* **2015**, *92*, No. 081104.
(80) Pavlyukh, Y.; Stefanucci, G.; van Leeuwen, R. Dynamically screened vertex correction to *GW*. *Phys. Rev. B* **2020**, *102*, No. 045121.
(81) Wang, Y.; Rinke, P.; Ren, X. Assessing the $G_0W_0\Gamma_0(1)$ Approach: Beyond G_0W_0 with Hedin's Full Second-Order Self-Energy Contribution. *J. Chem. Theory Comput.* **2021**, *17*, 5140−5154.
(82) Bruneval, F.; Förster, A. Fully Dynamic *G*3*W*2 Self-Energy for Finite Systems: Formulas and Benchmark. *J. Chem. Theory Comput.* **2024**, *20*, 3218−3230.
(83) Bruneval, F.; Förster, A.; Pavlyukh, Y. *GW*+2SOSEX Self-Energy Made Positive Semidefinite. *J. Chem. Theory Comput.* **2025**, *21*, 10223−10240.
(84) Northrup, J. E.; Hybertsen, M. S.; Louie, S. G. Theory of quasiparticle energies in alkali metals. *Phys. Rev. Lett.* **1987**, *59*, 819−822.
(85) Shirley, E. L. Self-consistent *GW* and higher-order calculations of electron states in metals. *Phys. Rev. B* **1996**, *54*, 7758−7764.
(86) Bruneval, F.; Sottile, F.; Olevano, V.; Del Sole, R.; Reining, L. Many-Body Perturbation Theory Using the Density-Functional Concept: Beyond the *GW* Approximation. *Phys. Rev. Lett.* **2005**, *94*, No. 186402.
(87) Shishkin, M.; Marsman, M.; Kresse, G. Accurate Quasiparticle Spectra from Self-Consistent *GW* Calculations with Vertex Corrections. *Phys. Rev. Lett.* **2007**, *99*, No. 246403.
(88) Schmidt, P. S.; Patrick, C. E.; Thygesen, K. S. Simple vertex correction improves *GW* band energies of bulk and two-dimensional crystals. *Phys. Rev. B* **2017**, *96*, No. 205206.
(89) Cunningham, B.; Grüning, M.; Pashov, D.; van Schilfgaarde, M. QS*GW*: Quasiparticle self-consistent *GW* with ladder diagrams in *W*. *Phys. Rev. B* **2023**, *108*, No. 165104.
(90) Del Sole, R.; Reining, L.; Godby, R. W. *GWΓ* approximation for electron self-energies in semiconductors and insulators. *Phys. Rev. B* **1994**, *49*, 8024−8028.
(91) Schindlmayr, A.; Godby, R. W. Systematic Vertex Corrections through Iterative Solution of Hedin's Equations Beyond the *GW* Approximation. *Phys. Rev. Lett.* **1998**, *80*, 1702−1705.
(92) Morris, A. J.; Stankovski, M.; Delaney, K. T.; Rinke, P.; García-González, P.; Godby, R. W. Vertex corrections in localized and extended systems. *Phys. Rev. B* **2007**, *76*, No. 155106.
(93) Romaniello, P.; Guyot, S.; Reining, L. The Self-Energy beyond *GW*: Local and Nonlocal Vertex Corrections. *J. Chem. Phys.* **2009**, *131*, No. 154111.
(94) Grüneis, A.; Kresse, G.; Hinuma, Y.; Oba, F. Ionization Potentials of Solids: The Importance of Vertex Corrections. *Phys. Rev. Lett.* **2014**, *112*, No. 096401.
(95) Kutepov, A. L. Electronic Structure of Na, K, Si, and LiF from Self-Consistent Solution of Hedin's Equations Including Vertex Corrections. *Phys. Rev. B* **2016**, *94*, No. 155101.
(96) Kuwahara, R.; Noguchi, Y.; Ohno, K. *GWΓ*+ Bethe-Salpeter equation approach for photoabsorption spectra: Importance of self-consistent *GWΓ* calculations in small atomic systems. *Phys. Rev. B* **2016**, *94*, No. 121116.
(97) Hung, L.; Bruneval, F.; Baishya, K.; Ogut, S. Benchmarking the *GW* Approximation and Bethe-Salpeter Equation for Groups IB and

IIB Atoms and Monoxides. *J. Chem. Theory Comput.* **2017**, *13*, 2135−2146.
(98) Maggio, E.; Kresse, G. *GW* Vertex Corrected Calculations for Molecular Systems. *J. Chem. Theory Comput.* **2017**, *13*, 4765−4778.
(99) Ma, H.; Govoni, M.; Gygi, F.; Galli, G. A Finite-Field Approach for *GW* Calculations beyond the Random Phase Approximation. *J. Chem. Theory Comput.* **2019**, *15*, 154−164.
(100) Tal, A.; Chen, W.; Pasquarello, A. Vertex function compliant with the Ward identity for quasiparticle self-consistent calculations beyond *GW*. *Phys. Rev. B* **2021**, *103*, L161104.
(101) Förster, A.; Visscher, L. Exploring the Statically Screened G_3W_2 Correction to the *GW* Self-Energy: Charged Excitations and Total Energies of Finite Systems. *Phys. Rev. B* **2022**, *105*, No. 125121.
(102) Rohlfing, M. Approximate spatiotemporal structure of the vertex function $\Gamma(1,2;\ 3)$ in many-body perturbation theory. *Phys. Rev. B* **2023**, *108*, No. 195207.
(103) Weng, G.; Mallarapu, R.; Vlček, V. Embedding Vertex Corrections in GW Self-Energy: Theory, Implementation, and Outlook. *Chem. Phys.* **2023**, *158*, No. 144105.
(104) Wen, M.; Abraham, V.; Harsha, G.; Shee, A.; Whaley, K. B.; Zgid, D. Comparing Self-Consistent *GW* and Vertex-Corrected G_0W_0 ($G_0W_0\Gamma$) Accuracy for Molecular Ionization Potentials. *J. Chem. Theory Comput.h* **2024**, *20*, 3109−3120.
(105) Vacondio, S.; Varsano, D.; Ruini, A.; Ferretti, A. Going Beyond the *GW* Approximation Using the Time-Dependent Hartree−Fock Vertex. *J. Chem. Theory Comput.* **2024**, *20*, 4718−4737.
(106) Förster, A.; Bruneval, F. Why Does the *GW* Approximation Give Accurate Quasiparticle Energies? The Cancellation of Vertex Corrections Quantified. *J. Phys. Chem. Lett.* **2024**, *15*, 12526−12534.
(107) Patterson, C. H. Molecular Ionization Energies from *GW* and Hartree−Fock Theory: Polarizability, Screening, and Self-Energy Vertex Corrections. *J. Chem. Theory Comput.* **2024**, *20*, 7479−7493.
(108) Förster, A. Beyond Quasi-Particle Self-Consistent *GW* for Molecules with Vertex Corrections. *J. Chem. Theory Comput.* **2025**, *21*, 1709−1721.
(109) Kutepov, A. L. Spatial non-locality of electronic correlations beyond *GW* approximation. *J. Phys. Cond. Mater.* **2021**, *33*, No. 485601.
(110) Winter, J. Study of core excitations in one-particle and one-holf nuclei by means of the six-point Green function. *Nucl. Phys. A* **1972**, *194*, 535−551.
(111) Cederbaum, L. S. Non-single-particle excitations in finite Fermi systems. *J. Chem. Phys.* **1975**, *62*, 2160−2170.
(112) Stefanucci, G.; Pavlyukh, Y.; Uimonen, A.-M.; van Leeuwen, R. Diagrammatic expansion for positive spectral functions beyond *GW*: Application to vertex corrections in the electron gas. *Phys. Rev. B* **2014**, *90*, No. 115134.
(113) Uimonen, A.-M.; Stefanucci, G.; Pavlyukh, Y.; van Leeuwen, R. Diagrammatic expansion for positive density-response spectra: Application to the electron gas. *Phys. Rev. B* **2015**, *91*, No. 115104.
(114) Pavlyukh, Y.; Uimonen, A.-M.; Stefanucci, G.; van Leeuwen, R. Vertex Corrections for Positive-Definite Spectral Functions of Simple Metals. *Phys. Rev. Lett.* **2016**, *117*, No. 206402.
(115) Schirmer, J. Beyond the Random-Phase Approximation: a new Approximation Scheme for the Polarization Propagator. *Phys. Rev. A* **1982**, *26*, 2395−2416.
(116) Schirmer, J.; Cederbaum, L. S.; Walter, O. New Approach to the One-Particle Green's Function for Finite Fermi Systems. *Phys. Rev. A* **1983**, *28*, 1237.
(117) Schirmer, J. *Many-Body Methods for Atoms, Molecules and Clusters*; Springer: 2018.
(118) Riva, G.; Romaniello, P.; Berger, J. A. Multichannel Dyson Equation: Coupling Many-Body Green's Functions. *Phys. Rev. Lett.* **2023**, *131*, No. 216401.
(119) Riva, G.; Romaniello, P.; Berger, J. A. Derivation and Analysis of the Multichannel Dyson Equation. *Phys. Rev. B* **2024**, *110*, No. 115140.
(120) Romaniello, P.; Berger, J. A. Direct and inverse photoemission spectra from the screened multichannel Dyson equation. 2026; https://arxiv.org/abs/2603.27329.
(121) Bintrim, S. J.; Berkelbach, T. C. Full-frequency *GW* without frequency. *J. Chem. Phys.* **2021**, *154*, No. 041101.
(122) Monino, E.; Loos, P.-F. Unphysical discontinuities, intruder states and regularization in *GW* methods. *J. Chem. Phys.* **2022**, *156*, No. 231101.
(123) Quintero-Monsebaiz, R.; Monino, E.; Marie, A.; Loos, P.-F. Connections between many-body perturbation and coupled-cluster theories. *J. Chem. Phys.* **2022**, *157*, No. 231102.
(124) Tölle, J.; Chan, G. K.-L. Exact relationships between the *GW* approximation and equation-of-motion coupled-cluster theories through the quasi-boson formalism. *J. Chem. Phys.* **2023**, *158*, No. 124123.
(125) Scott, C. J. C.; Backhouse, O. J.; Booth, G. H. A "moment-conserving" reformulation of *GW* theory. *J. Chem. Phys.* **2023**, *158*, No. 124102.
(126) Marie, A.; Loos, P.-F. A Similarity Renormalization Group Approach to Green's Function Methods. *J. Chem. Theory Comput.* **2023**, *19*, 3943−3957.
(127) Loos, P. F. *QuAcK: a software for emerging quantum electronic structure methods*. 2019; https://github.com/pfloos/QuAcK, https://github.com/pfloos/QuAcK.
(128) Sun, Q.; Berkelbach, T. C.; Blunt, N. S.; Booth, G. H.; Guo, S.; Li, Z.; Liu, J.; McClain, J. D.; Sayfutyarova, E. R.; Sharma, S.; Wouters, S.; Chan, G. K.-L. PySCF: the Python-based simulations of chemistry framework. *WIREs Comput. Mol. Sci.* **2018**, *8*, No. e1340.
(129) Sun, Q.; et al. Recent developments in the PySCF program package. *J. Chem. Phys.* **2020**, *153*, No. 024109.
(130) Marie, A.; Loos, P.-F. Parquet theory for molecular systems: Formalism and static kernel parquet approximation. *J. Chem. Phys.* **2025**, *163*, No. 194115.
(131) Bruneval, F.; Rangel, T.; Hamed, S. M.; Shao, M.; Yang, C.; Neaton, J. B. Molgw 1: Many-Body Perturbation Theory Software for Atoms, Molecules, and Clusters. *Comput. Phys. Commun.* **2016**, *208*, 149−161.
(132) von Niessen, W.; Schirmer, J.; Cederbaum, L. Computational methods for the one-particle Green's function. *Comput. Phys. Rep.* **1984**, *1*, 57−125.
(133) Schirmer, J.; Trofimov, A. B.; Stelter, G. A non-Dyson third-order approximation scheme for the electron propagator. *J. Chem. Phys.* **1998**, *109*, 4734−4744.
(134) Trofimov, A. B.; Stelter, G.; Schirmer, J. Electron Excitation Energies Using a Consistent Third-Order Propagator Approach: Comparison with Full Configuration Interaction and Coupled Cluster Results. *J. Chem. Phys.* **2002**, *117*, 6402−6410.
(135) Schirmer, J. Closed-Form Intermediate Representations of Many-Body Propagators and Resolvent Matrices. *Phys. Rev. A* **1991**, *43*, 4647−4659.
(136) Mertins, F.; Schirmer, J. Algebraic propagator approaches and intermediate-state representations. I. The biorthogonal and unitary coupled-cluster methods. *Phys. Rev. A* **1996**, *53*, 2140−2152.
(137) Mertins, F.; Schirmer, J.; Tarantelli, A. Algebraic propagator approaches and intermediate-state representations. II. The equation-of-motion methods for N, N1, and N2 electrons. *Phys. Rev. A* **1996**, *53*, 2153−2168.
(138) Trofimov, A. B.; Schirmer, J. Molecular Ionization Energies and Ground- and Ionic-State Properties Using a Non-Dyson Electron Propagator Approach. *J. Chem. Phys.* **2005**, *123*, No. 144115.
(139) Dreuw, A.; Papapostolou, A.; Dempwolff, A. L. Algebraic Diagrammatic Construction Schemes Employing the Intermediate State Formalism: Theory, Capabilities, and Interpretation. *J. Phys. Chem. A* **2023**, *127*, 6635−6646.
(140) Banerjee, S.; Sokolov, A. Y. Algebraic Diagrammatic Construction Theory for Simulating Charged Excited States and Photoelectron Spectra. *J. Chem. Theory Comput.* **2023**, *19*, 3037−3053.

(141) Loos, P.-F.; Tölle, J. From Full Dynamic to Pure Static: A Family of *GW*-Based Approximations. 2026; https://arxiv.org/abs/2604.08350.
(142) Bruneval, F. Improved density matrices for accurate molecular ionization potentials. *Phys. Rev. B* **2019**, *99*, No. 041118.
(143) Bruneval, F. Assessment of the linearized *GW* density matrix for molecules. *J. Chem. Theory Comput.* **2019**, *15*, 4069−4078.
(144) Bruneval, F.; Rodriguez-Mayorga, M.; Rinke, P.; Dvorak, M. Improved one-shot total energies from the linearized *GW* density matrix. *J. Chem. Theory Comput.* **2021**, *17*, 2126−2136.
(145) Sokolov, A. Y. Multi-Reference Algebraic Diagrammatic Construction Theory for Excited States: General Formulation and First-Order Implementation. *J. Chem. Phys.* **2018**, *149*, No. 204113.
(146) Chatterjee, K.; Sokolov, A. Y. Second-Order Multireference Algebraic Diagrammatic Construction Theory for Photoelectron Spectra of Strongly Correlated Systems. *J. Chem. Theory Comput.* **2019**, *15*, 5908−5924.
(147) Chatterjee, K.; Sokolov, A. Y. Extended Second-Order Multireference Algebraic Diagrammatic Construction Theory for Charged Excitations. *J. Chem. Theory Comput.* **2020**, *16*, 6343−6357.
(148) Banerjee, S.; Sokolov, A. Y. Third-Order Algebraic Diagrammatic Construction Theory for Electron Attachment and Ionization Energies: Conventional and Green's Function Implementation. *J. Chem. Phys.* **2019**, *151*, No. 224112.
(149) Banerjee, S.; Sokolov, A. Y. Non-Dyson Algebraic Diagrammatic Construction Theory for Charged Excitations in Solids. *J. Chem. Theory Comput.* **2022**, *18*, 5337−5348.
(150) Crawford, T. D.; Schaefer, H. F. *Reviews in Computational Chemistry*; John Wiley & Sons, Ltd: 2000; pp 33−136.
(151) Piecuch, P.; Kowalski, K.; Pimienta, I. S. O.; Mcguire, M. J. Recent advances in electronic structure theory: Method of moments of coupled-cluster equations and renormalized coupled-cluster approaches. *Int. Rev. Phys. Chem.* **2002**, *21*, 527−655.
(152) Bartlett, R. J.; Musiał, M. Coupled-Cluster Theory in Quantum Chemistry. *Rev. Mod. Phys.* **2007**, *79*, 291−352.
(153) Shavitt, I.; Bartlett, R. J. *Many-Body Methods in Chemistry and Physics: MBPT and Coupled-Cluster Theory*; Cambridge Molecular Science, Cambridge University Press: 2009.
(154) Bartlett, R. J. Perspective on Coupled-cluster Theory. The evolution toward simplicity in quantum chemistry. *Phys. Chem. Chem. Phys.* **2024**, *26*, 8013−8037.
(155) Prasad, M. D.; Pal, S.; Mukherjee, D. Some aspects of self-consistent propagator theories. *Phys. Rev. A* **1985**, *31*, 1287−1298.
(156) Hättig, C.; Jensen, H. A. Structure optimizations for excited states with correlated secondorder methods: CC2 and ADC(2). *Advances in Quantum Chemistry* **2005**, *50*, 37−60.
(157) Liu, J.; Asthana, A.; Cheng, L.; Mukherjee, D. Unitary coupled-cluster based self-consistent polarization propagator theory: A third-order formulation and pilot applications. *J. Chem. Phys.* **2018**, *148*, No. 244110.
(158) Hodecker, M.; Rehn, D. R.; Dreuw, A. Hermitian second-order methods for excited electronic states: Unitary coupled cluster in comparison with algebraic−diagrammatic construction schemes. *J. Chem. Phys.* **2020**, *152*, No. 094106.
(159) Hodecker, M.; Thielen, S. M.; Liu, J.; Rehn, D. R.; Dreuw, A. Third-Order Unitary Coupled Cluster (UCC3) for Excited Electronic States: Efficient Implementation and Benchmarking. *J. Chem. Theory Comput.* **2020**, *16*, 3654−3663.
(160) Lange, M. F.; Berkelbach, T. C. On the Relation between Equation-of-Motion Coupled-Cluster Theory and the *GW* Approximation. *J. Chem. Theory. Comput.* **2018**, *14*, 4224−4236.
(161) Tölle, J. Fully Analytic G_0W_0 Nuclear Gradients. *J. Phys. Chem. Lett.* **2025**, *16*, 3672−3678.
(162) Tölle, J.; Kitsaras, M.-P.; Loos, P.-F. Fully Analytic Nuclear Gradients for the Bethe−Salpeter Equation. *J. Phys. Chem. Lett.* **2025**, *16*, 11134−11143.
(163) Kitsaras, M.-P.; Tölle, J.; Loos, P.-F. Analytic G_0W_0 gradients based on a double-similarity transformation equation-of-motion coupled-cluster treatment. *J. Chem. Phys.* **2026**, *164*, No. 044122.
(164) Coveney, C. J. N.; Tew, D. P. Diagrammatic theory of the irreducible coupled-cluster self-energy. *Phys. Rev. B* **2025**, *112*, No. 045104.
(165) Coveney, C. J. N. Uncovering Relationships between the Electronic Self-Energy and Coupled-Cluster Doubles Theory. *J. Phys. Chem. A* **2025**, *129*, 8689−8698.
(166) Coveney, C. J. N.; Tew, D. P. Non-Hermitian Green's function theory with *N*-body interactions: The coupled-cluster similarity transformation. *Phys. Rev. Res.* **2026**, *8*, No. 013322.
(167) Tölle, J.; Kitsaras, M.-P.; Irmler, A.; Grüneis, A.; Loos, P.-F. Connection between GW and Extended Coupled Cluster. *J. Chem. Theory Comput.* **2026**, *0*, null.

https://doi.org/10.1021/acs.jpclett.6c01904
J. Phys. Chem. Lett. 2026, 17, 8541−8551